# The NIKA2 Sunyaev Zel'dovich Large Program: cluster mass estimation

Miren Muñoz Echeverría, LPSC Grenoble,
on behalf of the NIKA2 collaboration


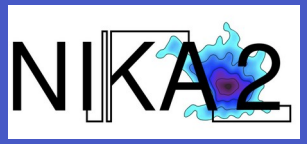


32nd Rencontres de Blois | 17 - 22 October, 2021

# Cosmology with galaxy clusters

**Galaxy clusters**: largest gravitationally bound objects in the universe
Created by gravitational collapse in the peaks of the matter density at the intersection of the filaments of the cosmic web

Mass ~ $10^{13}$ - $10^{16}$ $M_{sun}$

Temperature ≥ $10^{7}$ K (~ 1 keV)

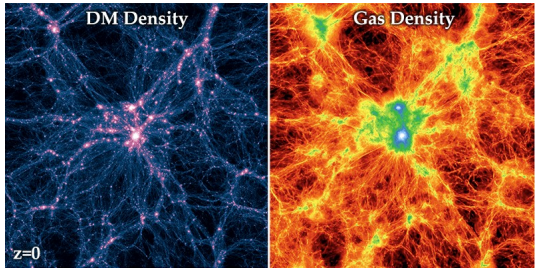

[Illustris Collaboration]

**Composition**:
- 85% dark matter
- 12% hot ionised gas = the Intra-Cluster Medium (ICM)
- 3% galaxies

Clusters as **cosmological probes**

- tracers of the matter in the universe $f_{\rm gas} \sim \frac{\Omega_{\rm b}}{\Omega_{\rm m}}$

- cluster counts with respect to **mass and redshift distribution**

$$\frac{d^2N}{dMdz} \sim \int d\Omega \frac{d^2V}{dzd\Omega}\frac{dn}{dM}$$

Dependent of the evolution of the universe and the structure formation rate

# Cluster observables and mass estimates

Optical/Infrared:
Stellar light of the galaxies

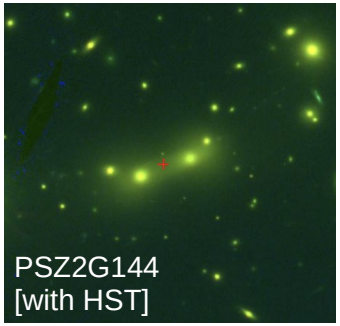


- Lensing of background galaxies
- Galaxy members richness and velocity dispersion

→ Different **mass** estimates

X-ray:
the hot ICM emission in X-ray

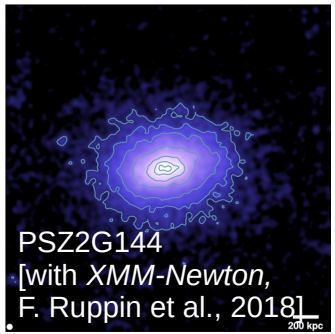


- Spectral line emission of metals
  → Temperature
- Bremsstrahlung of electrons
  → Electron density

Millimeter wavelengths:
Sunyaev-Zel'dovich (SZ) effect
from hot electrons in the ICM

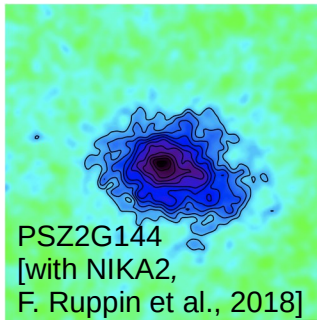


→ Thermal pressure of the ICM

→ **Hydrostatic mass** estimates from X-ray and SZ

**Different mass estimates** affected by **different systematic** uncertainties. **Combining observables** may help building a consistent picture of the cluster physics to gain accuracy on the mass estimates

# The Sunyaev-Zel'dovich effect

Thermal Sunyaev-Zel'dovich (**tSZ**) effect:
the inverse Compton scattering of CMB photons on the hot electrons of the ICM, which causes a spectral distortion of the CMB, independent of the redshift

[Courtesy of Florian Ruppin]

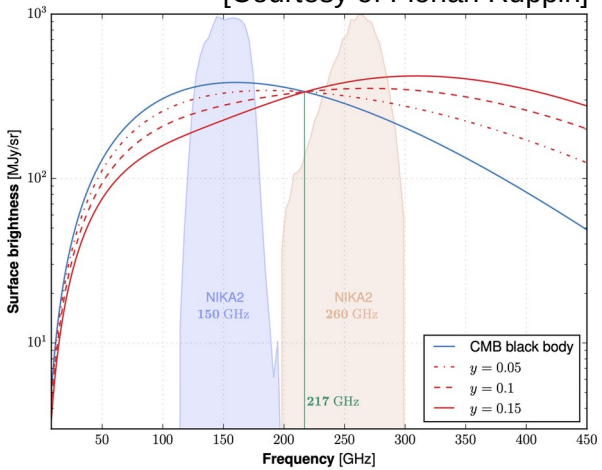


Relative variation in CMB intensity:

$$\left[\frac{\Delta I}{I_0}\right]_{SZ} = y\, f(\nu, T_e)$$

Spectral dependence of the SZ effect

CMB specific intensity

$$y = \frac{\sigma_T}{m_e c^2} \int P_e \, dl$$

The amplitude of the tSZ effect or **Compton parameter: pressure** of the ICM integrated along the line-of-sight

Abel 2319 galaxy cluster [Planck]

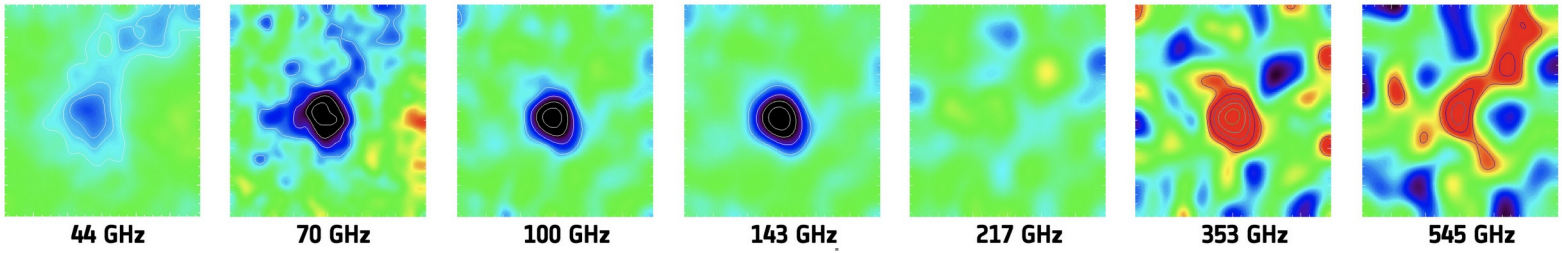

NIKA2 is a millimeter continuum camera of 2 900 Kinetic Inductance Detectors (KID) installed at the IRAM 30-meter telescope, and operating since 2017

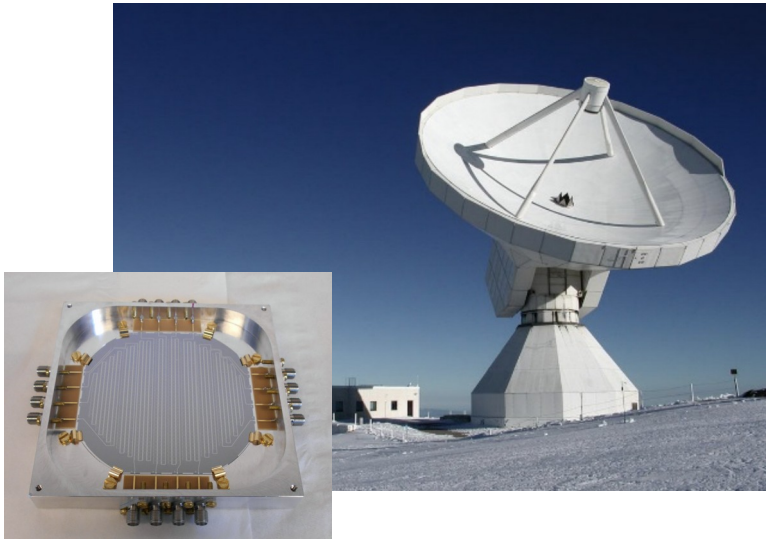

**Suited** for observing the **SZ** effect:

- Operating at **150** and **260 GHz**: observe the distortion
- **High angular resolution** (18'' and 12''): resolved maps of high redshift clusters
- 6.5' field of view: map the entire cluster
- High sensitivity: detect the weak signal of clusters

[Courtesy of Florian Ruppin]

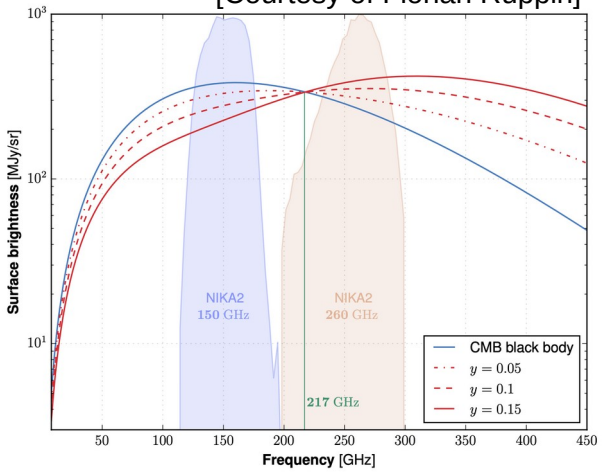

# The NIKA2 Sunyaev-Zel'dovich Large Program (LPSZ)

PSZ2G144 [F. Ruppin et al., 2018]

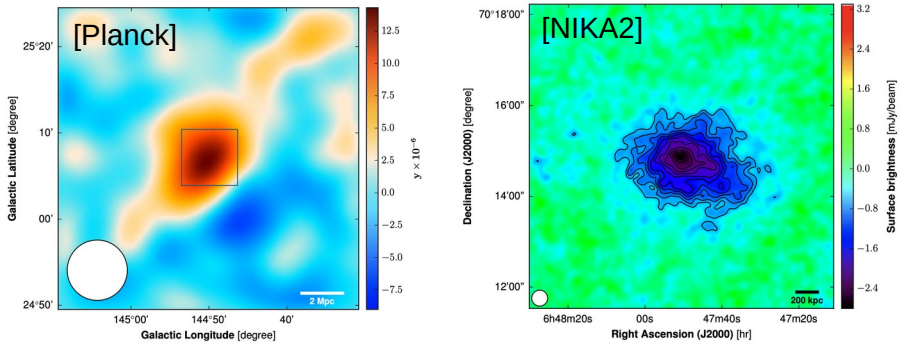


Status before LPSZ:
Catalogues of several thousands of clusters detected via the SZ effect with lower resolution instruments

→ need to resolve high redshift clusters to study their physical properties and masses

The **LPSZ**:
Study of 45 high redshift galaxy clusters selected in mass and redshift from Planck and ACT

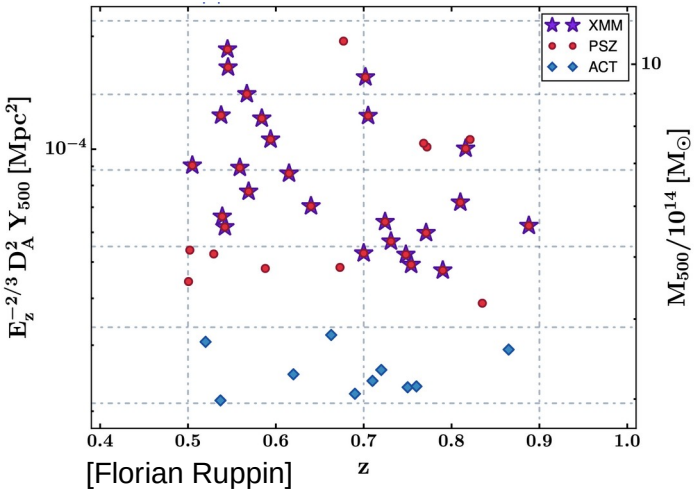


Main **goals**:

- Thermodynamical **properties of the ICM**
- **Relation** between the **tSZ observable ($Y_{500}$) and the mass ($M_{500}$)**
- Probe the **low-mass and high-redshift clusters**

With:

- tSZ measurements with NIKA2
- X-ray data from *XMM-Newton*

$P_e(r)$

$n_e(r), T_e(r)$

$M_{HSE}(r)$

# The galaxy cluster CL J1226.9+3332

Highest redshift cluster of the LPSZ: z ~ 0.9

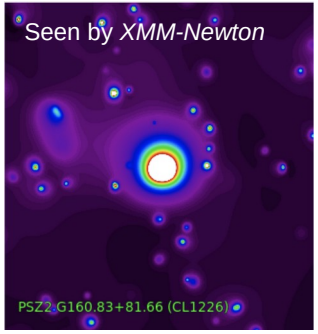


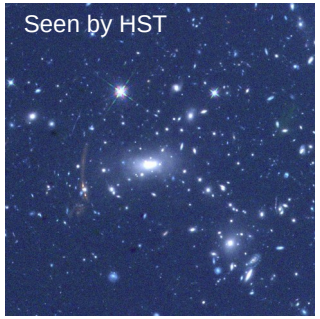


Maps obtained with the NIKA2 collaboration's pipeline:
- Calibration
- Atmospheric and electronic contamination removal → Pipeline filtering
- Projection into sky map

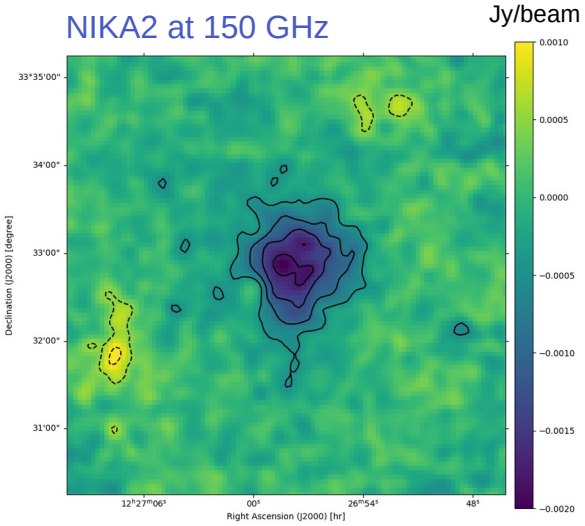


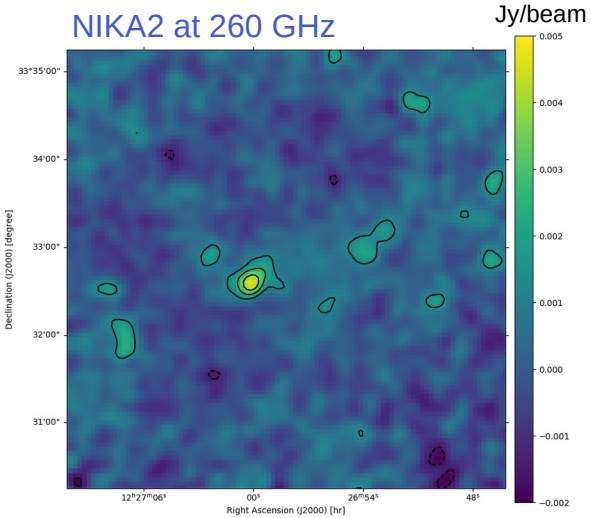


5' maps, with a 10'' FWHM smooth. Contours are multiples of 3σ starting from 3σ
The SZ signal is contaminated by the positive signal of galaxies

# Pressure profile determination with NIKA2

MCMC fit of electronic **pressure profile model** and point sources to the NIKA2 150 GHz map
Using PANCO2 pipeline [F. Kéruzoré et al., *in prep*.]

Pressure profile model

Positive sources fluxes

$$\mathrm{MODEL}^{(x,y)}_{150GHz} = C^{(x,y)}_{150GHz} \left( \frac{\sigma_T}{m_e c^2} \int P_e dl \right)_{cluster} + \sum_{Sources} \mathrm{g}_{2D}(F_{150GHz},\ 17{,}7") + \mathrm{Zero}$$

Accounts for:

- instrumental and filtering effects
- conversion from Compton parameter ($y$) to surface brightness units

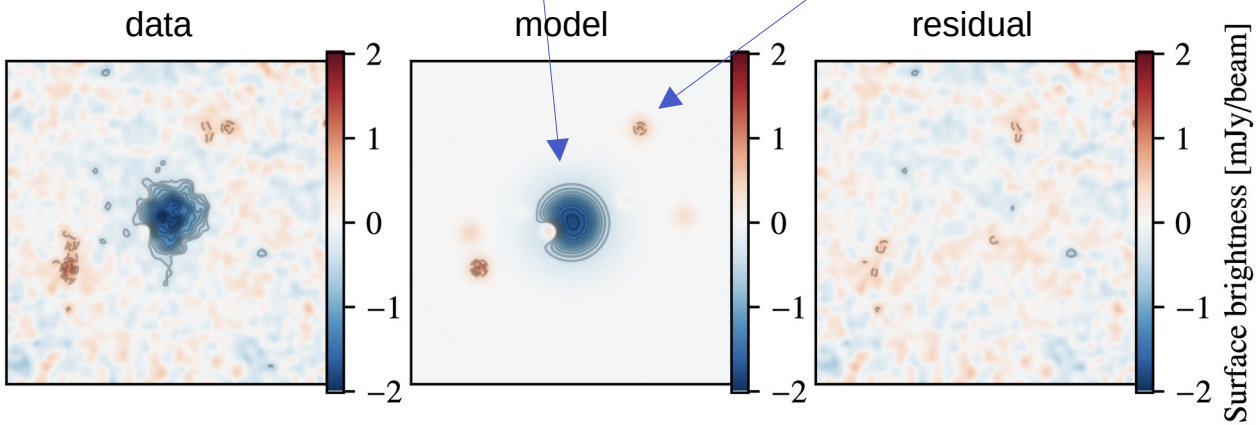

# Pressure profile of CL J1226.9+3332

We test the robustness of our estimate by:

- Fitting different pressure models

Radially binned

$$P_e(r) = P_i \left( \frac{r}{r_i} \right)^{-\alpha_i}$$

gNFW

$$P_e(r) = \frac{P_0}{\left(\frac{r}{r_p}\right)^c \left(1 + \left(\frac{r}{r_p}\right)^a\right)^{\frac{b-c}{a}}}$$

- Defining the filtering induced by the data processing differently

  2D: accounting for anisotropies in filtering
  1D: assuming isotropic filtering

Reconstructed pressure profiles for CL J1226.9+3332

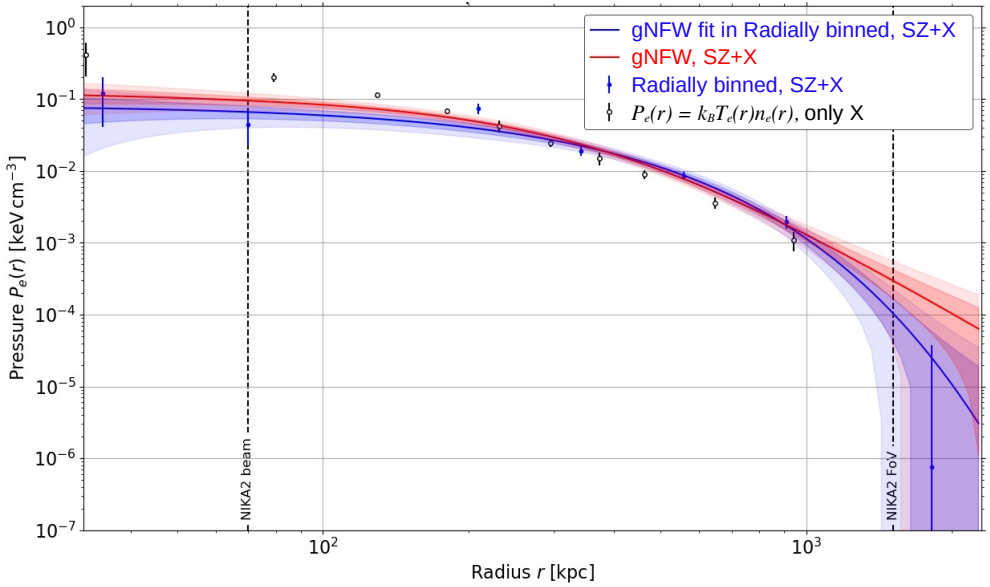


*Results assuming isotropic filtering (1D)

# Hydrostatic mass and SZ signal

Hydrostatic equilibrium hypothesis for galaxy clusters: pressure compensates the gravity

The hydrostatic mass inside a sphere of radius $r$ :

$$\mathrm{M_{HSE}}(< r) = -\frac{r^2}{G\mu m_p n_e(r)} \frac{dP(r)}{dr}$$

Thermal pressure of the ICM from the SZ effect

Electron density from X-rays

We compare cluster masses and SZ signal inside a virialized sphere, in the literature very often at $R_{500}$ :

$$500 = \frac{\langle \rho(r < R_{500}) \rangle}{\rho_c(z)}$$

Hydrostatic mass and SZ signal at $R_{500}$

$$\mathrm{M}_{500}^{\mathrm{HSE}} = \mathrm{M}^{\mathrm{HSE}}(r < R_{500})$$

$$\mathrm{Y}_{500} = \frac{\sigma_T}{m_e c^2 \mathcal{D}_{\mathrm{A}}^2} \int_0^{\mathrm{R}_{500}} P_e(r) 4\pi r^2 dr$$

# Hydrostatic mass of CL J1226.9+3332

Hydrostatic mass profile for CL J1226.9+3332

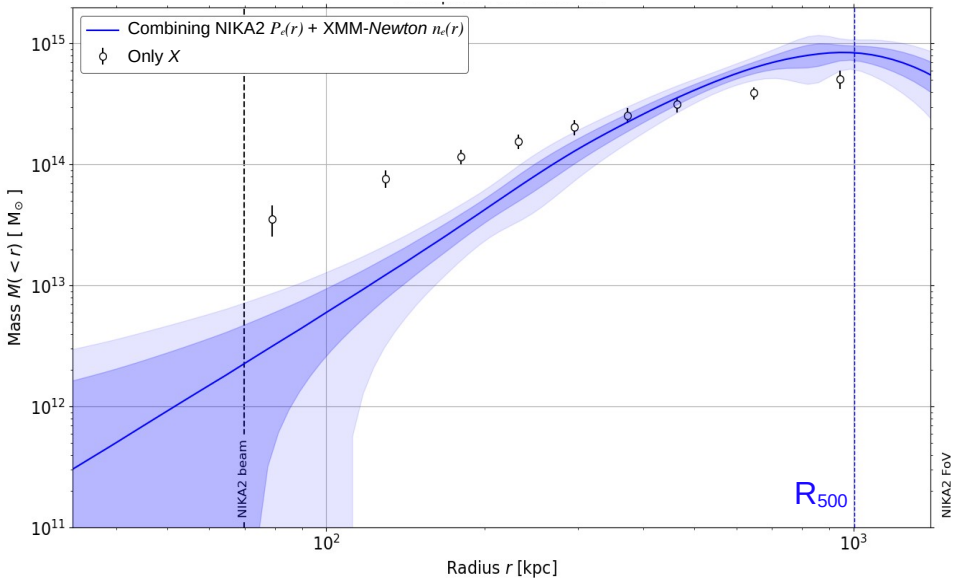


*Example from Radially binned pressure model assuming isotropic filtering (1D)

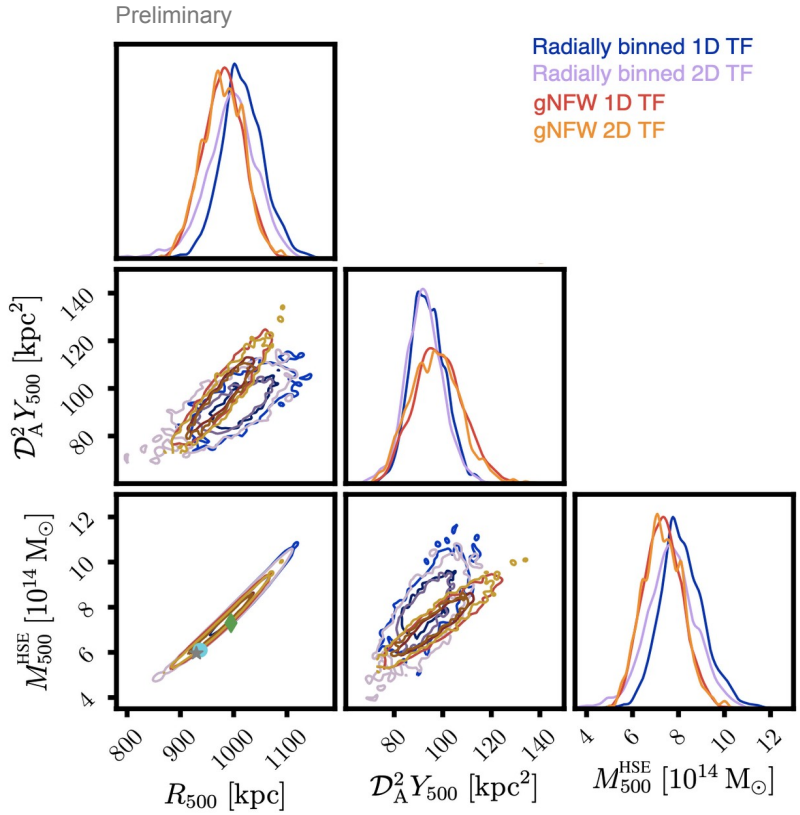


Tested systematic effects give robust hydrostatic mass estimates

# Lensing mass of CL J1226.9+3332

The CLASH dataset provides lensing **convergence maps** that can be converted into **mass density maps**
Convergence maps used here are the result of lensing raw data analysis described in Zitrin et al., 2015

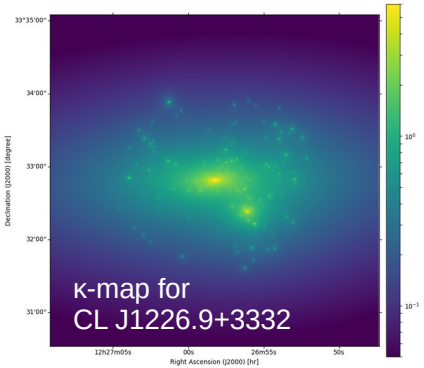


$$\kappa = \Sigma / \Sigma_{crit}$$

$\kappa$ : convergence, $\Sigma$ in critical density unities $\Sigma_{crit}$
$\Sigma$ : **surface mass density**
$\Sigma_{crit}$ : the density needed for strong lensing to occur

Fit $\Sigma$ to a projected density model using MCMC approach:

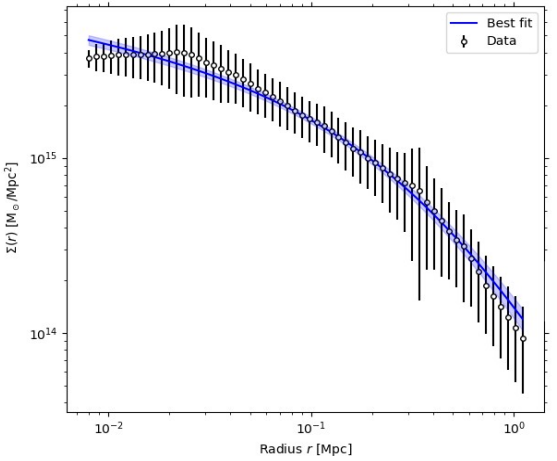


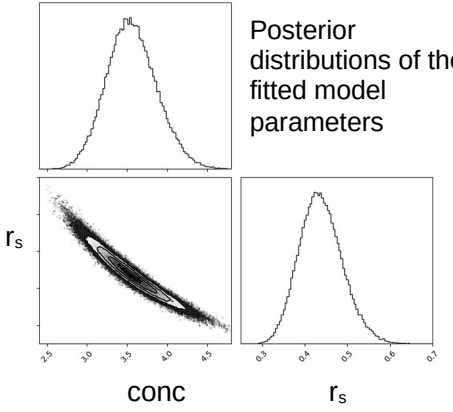


Lensing mass profile for CL J1226.9+3332

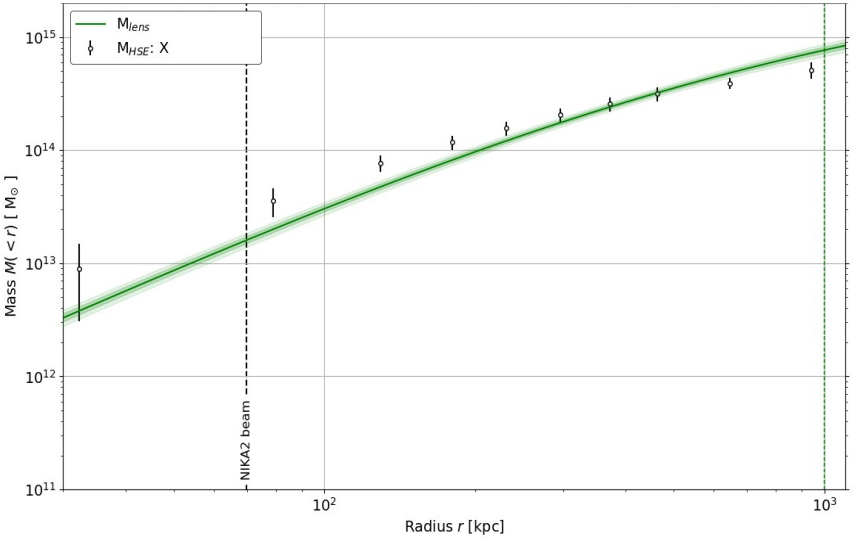

# Hydrostatic and lensing mass of galaxy clusters
# A combined NIKA-LPSZ-CLASH sample: convergence and SZ maps

CL J1226.9+3332 | PSZ2G144 | PSZ2G228 | PSZ2G045 | MACSJ1424 | MACSJ0717

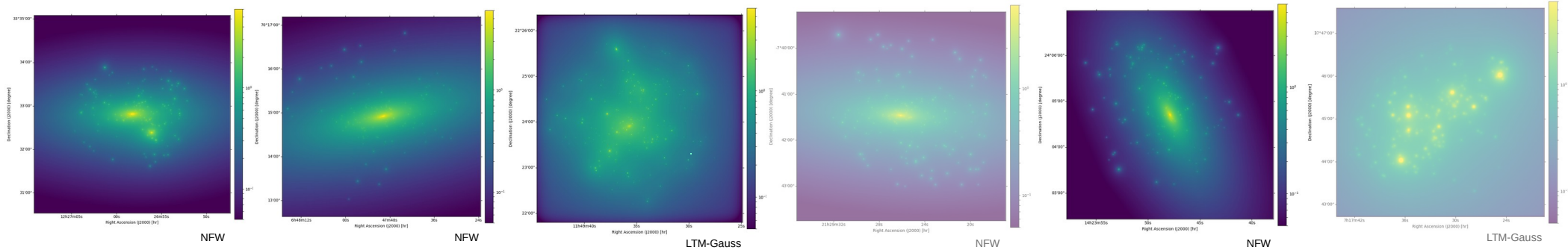


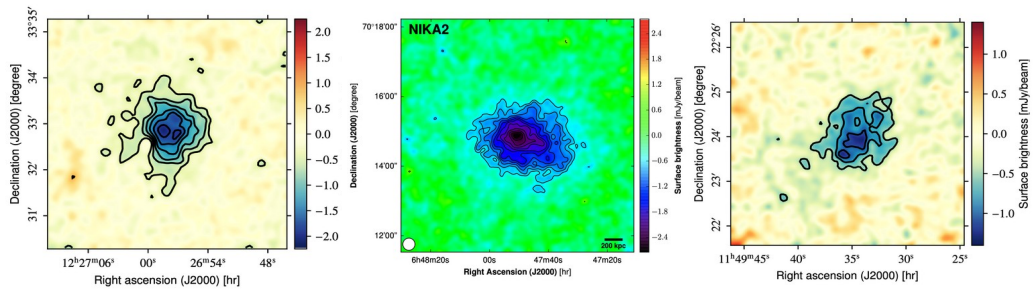


First Sunyaev-Zel'dovich mapping with the NIKA2 camera: Implication of cluster substructures for the pressure profile and mass estimate (Ruppin et al. 2018)

Ongoing analysis

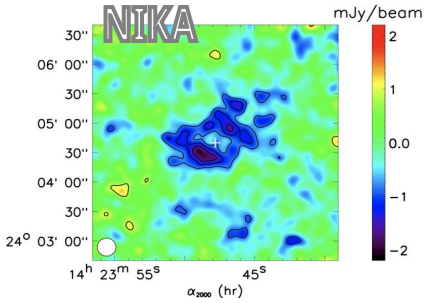


High angular resolution Sunyaev-Zel'dovich observations of MACS J1423.8+2404 with NIKA: Multiwavelength analysis (Adam et al. 2018)

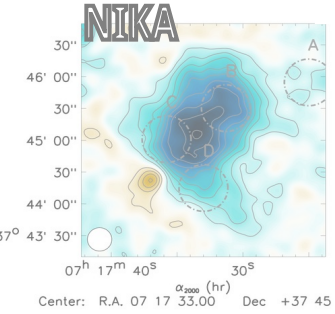


Mapping the kinetic Sunyaev-Zel'dovich effect toward MACS J0717.5+3745 with NIKA (Adam et al. 2016)

# Hydrostatic and lensing mass of galaxy clusters
# A combined NIKA-LPSZ-CLASH sample

For each cluster the marginalized $M_{500}$ distributions for hydrostatic and lensing estimates

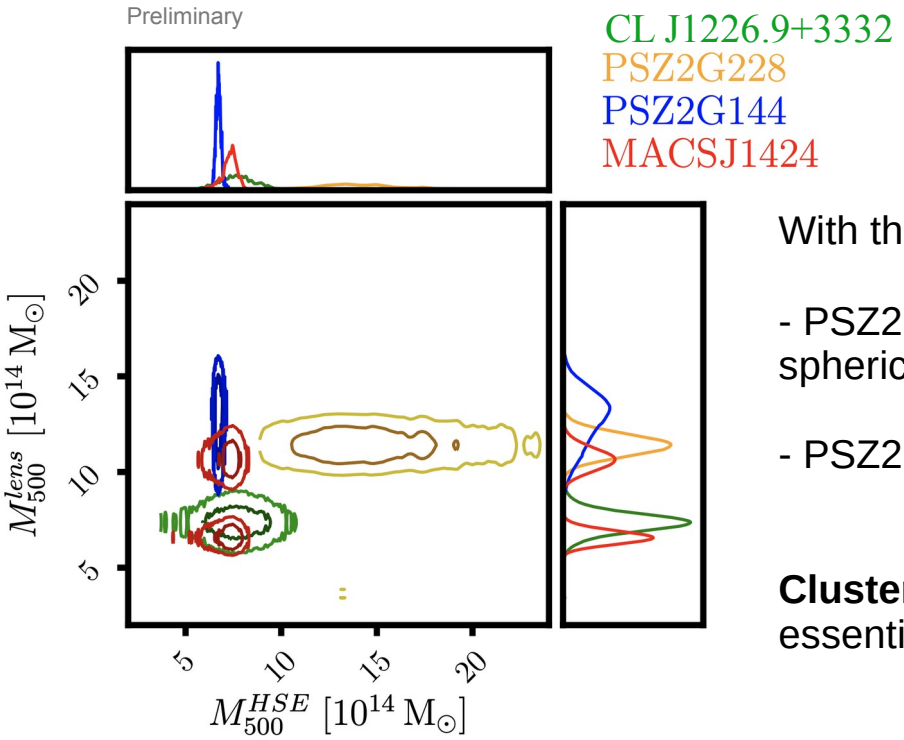


With this sample, we don't get a linear $M_{500}^{HSE}$ - $M_{500}^{lens}$ relation

- PSZ2G228 has a very complex morphology to be fitted with spherical models

- PSZ2G144 has a very good $M_{500}^{HSE}$ estimate compared to $M_{500}^{lens}$

**Clusters properties affect differently the mass estimates**: essential to compare the lensing and hydrostatic mass estimates

# Conclusions

The NIKA2 Sunyaev-Zel'dovich Large Program is well advanced:

- 30/45 clusters observed with high quality data
- Automatic analysis tools have been developed

This allows us to:

- Have good reconstructions of hydrostatic mass profiles combining NIKA2 and XMM-*Newton* data
- Characterize systematic effects on mass estimates

Combining LPSZ and CLASH data we can:

- Get the first hydrostatic to lensing mass bias in a combined sample at this redshift range ($0.5 < z < 0.9$)
- Study the mass dependence with clusters physical properties

# Backup slides

# Halo mass function

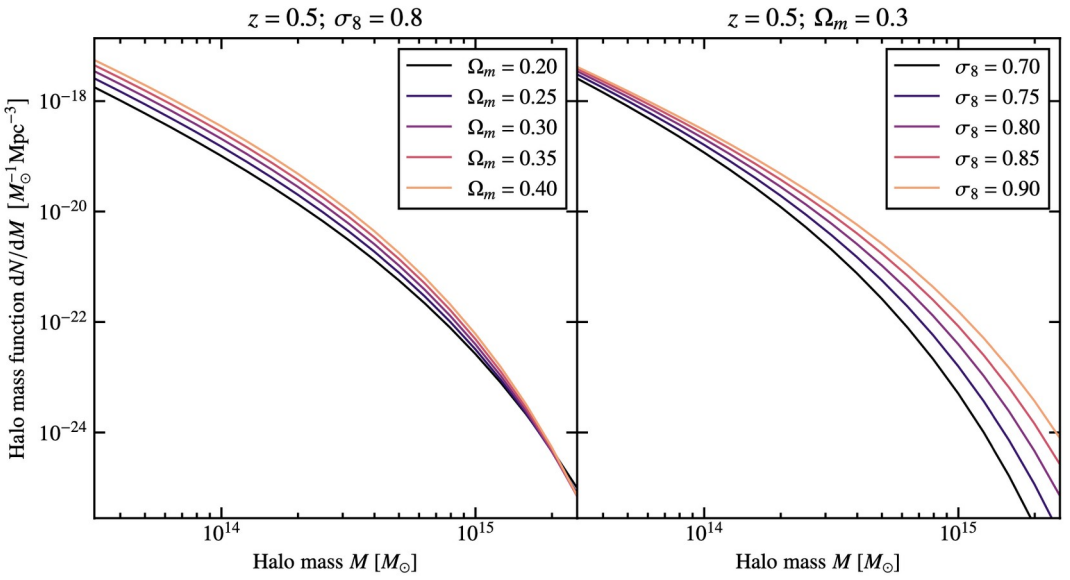


Figure 1.3 : Illustration de l'évolution de la fonction de masse avec les paramètres cosmologiques. La fonction de masse de Tinker *et al.* [32] est représentée pour différentes valeurs de $\Omega_m$ (*gauche*), et de $\sigma_8$ (*droite*). Le redshift est fixé à $z = 0.5$.

[Courtesy of Florian Kéruzoré]

# Hydrostatic bias

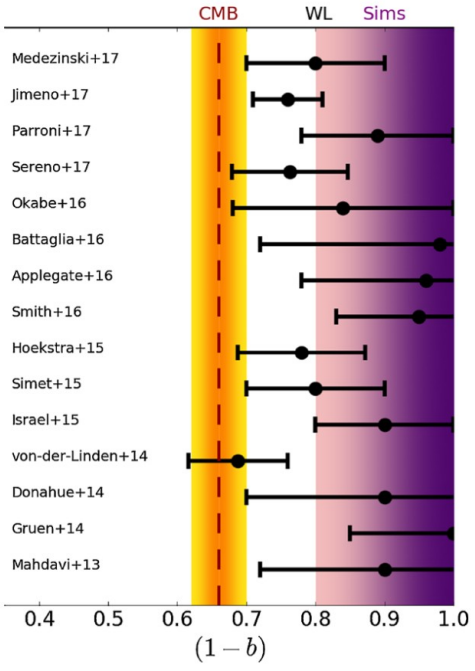


Figure 2.1 : Estimation du biais hydrostatique par comparaison de mesures de masse hydrostatique et par lentillage faible (voir section 2.2.1) pour différentes études (noir). La valeur nécessaire pour concilier les réultats du CMB et des amas de galaxies, mesurée par [51], est indiquée en orange. La région violette représente les valeurs de $(1-b)$ permises par plusieurs analyses d'amas simulés [52]. Figure extraite de [51].

[L. Salvati, et al. 2018]

# Cosmo params

[Courtesy of Florian Kéruzoré]

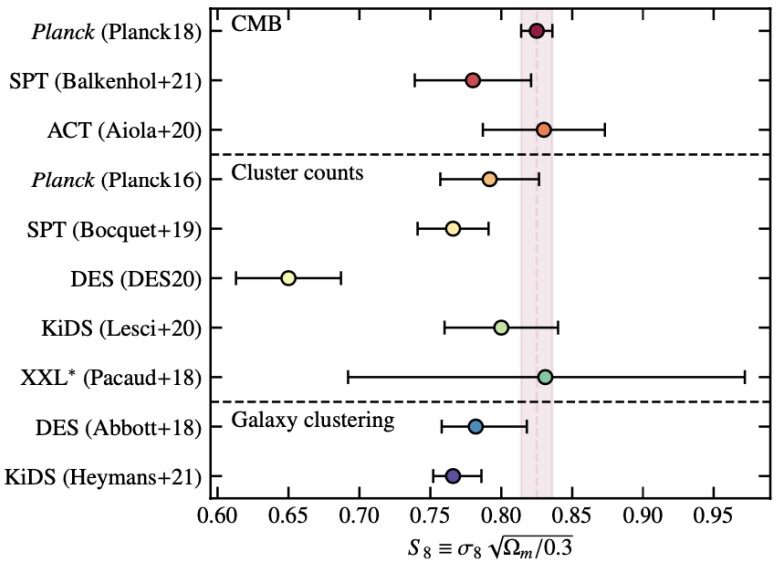


Figure 2.9 : Contrainte sur la combinaison de paramètres cosmologiques $S_8$ obtenues par différentes mesures du CMB (haut), de comptage d'amas (milieu), et de distribution de galaxies (bas). De haut en bas, les résultats sont issus de [13][119][120][100][99][103][107][102][121][122].
* : incertitudes estimées graphiquement.

# Observed clusters in mass and redshift

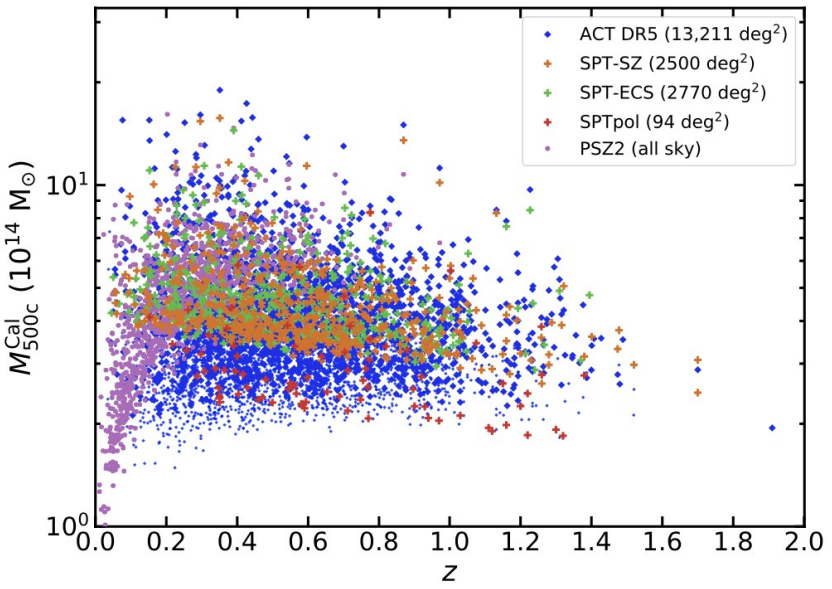


Figure 2.8 : Distribution dans le plan masse-redshift des amas détectés par les relevés ACT (bleu, [2]), SPT (orange [3], vert [4] et rouge [114]) et *Planck* (violet, [113]). Figure extraite de [2].

[M. Hilton et al., 2021]

# SZ effect formalism

[Courtesy of Florian Kéruzoré]

La dépendance spectrale de la distorsion peut être calculée à partir de l'équation de Kompaneets [81, 82] : pour un bain d'électrons non-relativistes ($k_B T_e \ll m_e c^2$) traversé par des photons de fréquence réduite $x_e \equiv h\nu/k_B T_e$, on a

$$\frac{\partial n}{\partial y} = \frac{1}{x_e^2}\frac{\partial}{\partial x_e}\left[x_e^4\left(\frac{\partial n}{\partial x_e} + n^2 + n\right)\right], \tag{2.8}$$

où $n$ est l'indice d'occupation des photons, défini pour une intensité spécifique $I_\nu$ à une fréquence $\nu$ comme

$$n \equiv \frac{I_\nu c^2}{2h\nu^3}, \tag{2.9}$$

et $y$ est le paramètre de Compton, défini comme

$$y \equiv \int \frac{k_B T_e}{m_e c^2}\,\mathrm{d}\tau_e \tag{2.10}$$

où $\tau_e \equiv n_e \sigma_T l$ est la profondeur optique[6] parcourue par les photons le long de la ligne de visée $l$ ; $n_e$ est la densité d'électrons, et $\sigma_T$ la section efficace de diffusion Thompson.
Cette équation peut alors aussi s'écrire

$$y = \int \frac{k_B T_e}{m_e c^2} n_e \sigma_T \,\mathrm{d}l = \frac{\sigma_T}{m_e c^2}\int k_B T_e\, n_e \,\mathrm{d}l. \tag{2.11}$$

Dans le cas de l'effet SZ, l'énergie des photons incidents est très faible par rapport à celle des électrons, soit $x_e \ll 1$ et donc $\partial n/\partial x_e \gg n, n^2$. L'équation (2.8) se simplifie alors, et en y injectant l'expression d'un spectre de corps noir pour les photons du CMB, on trouve l'expression de la variation d'intensité spécifique due à l'effet tSZ :

$$\frac{\Delta I_\nu^{\mathrm{tSZ}}}{I_0} = y \times \frac{x^4 e^x}{(e^x - 1)^2}\left[x\coth(x/2) - 4\right]\left[1 + \delta_r(x, T)\right], \tag{2.12}$$

# Transfer function: raw data analysis-induced filtering

1D

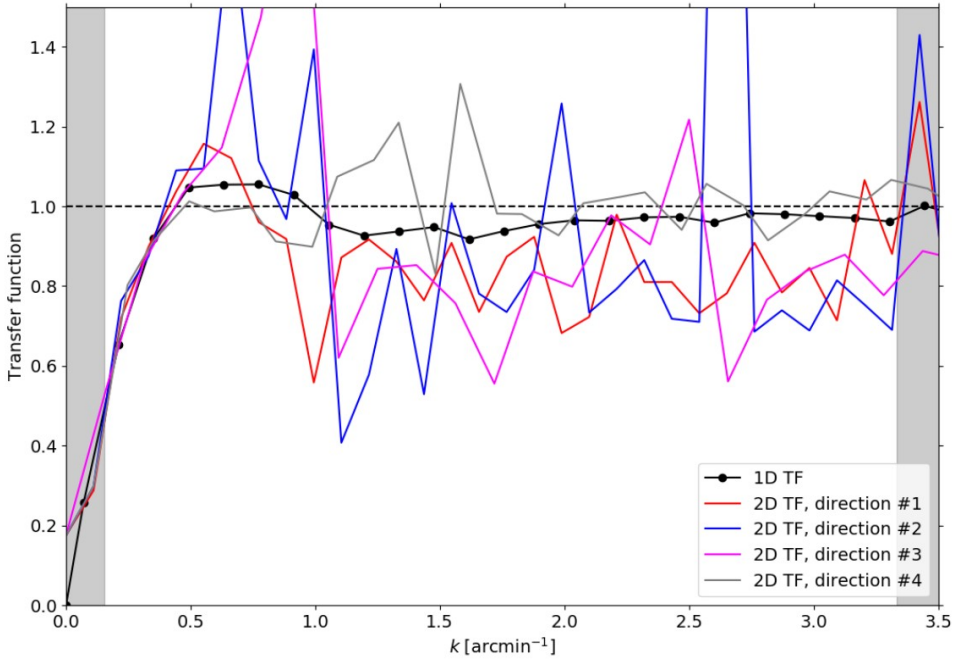


2D

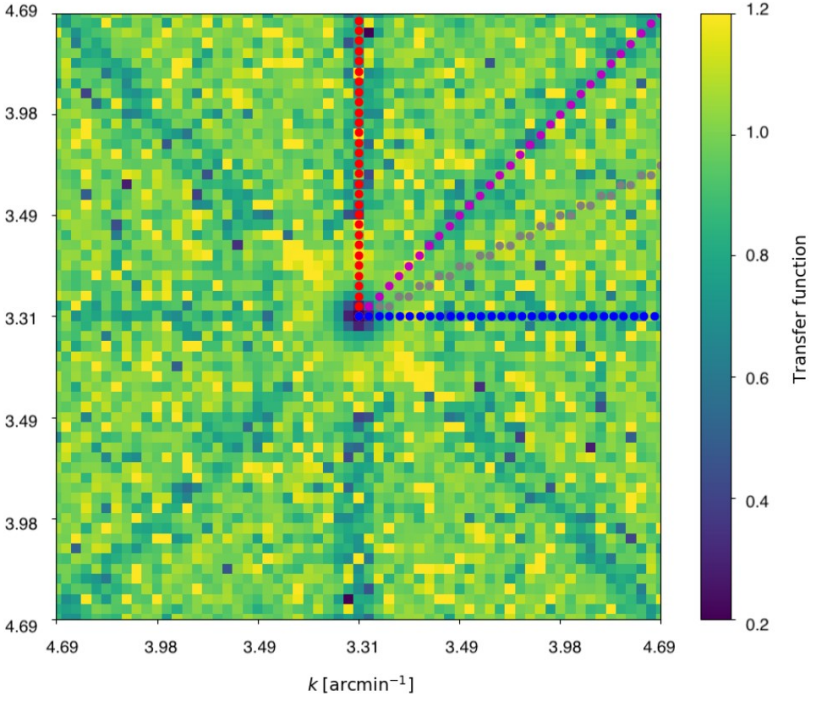

# Fit of SZ maps to pressure models

## CLJ1226.9+3332

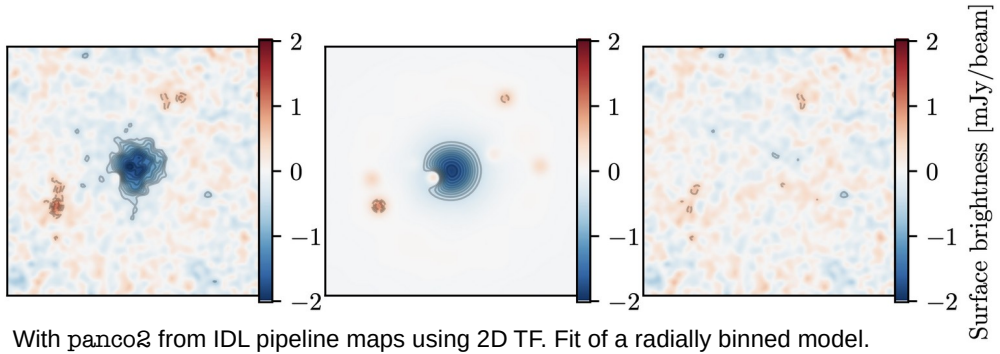


With panco2 from IDL pipeline maps using 2D TF. Fit of a radially binned model.

## PSZ2G228

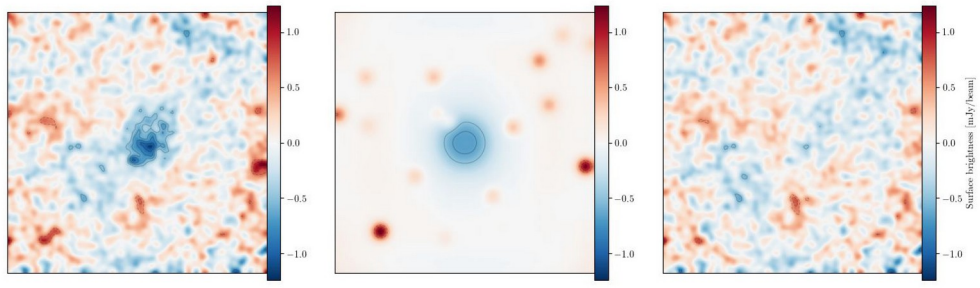

With panco2 from IDL pipeline maps using 2D TF. Fit of a radially binned model.
Big presence of contaminants and weaker cluster than expected.

## PSZ2G144

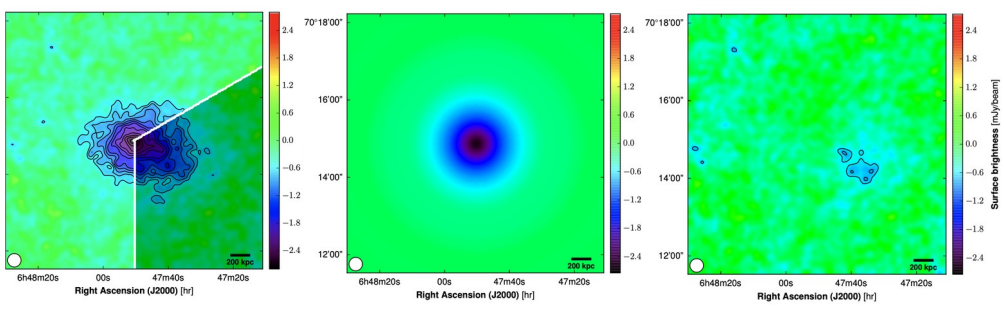


(Ruppin et al. 2018)
Residual over-pressure from spherical fit.

## MACSJ1424

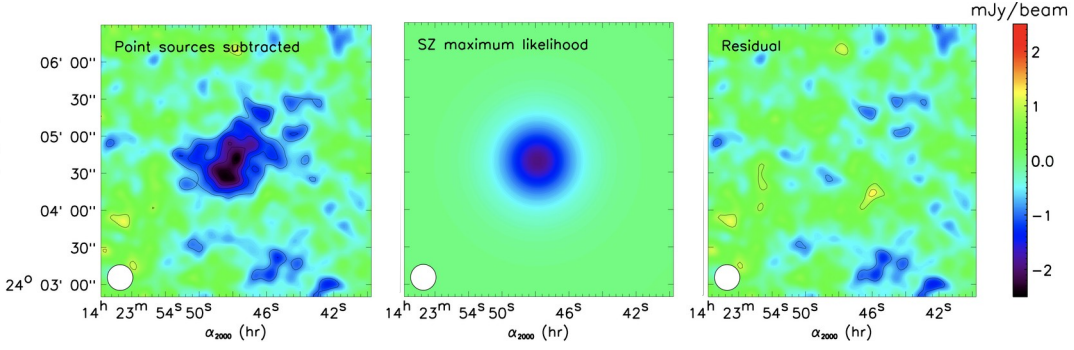


(Adam et al. 2018)
Central point source, subtracted for the fit of the pressure.

# Fit of κ-maps to density models

**CLJ1226.9+3332**

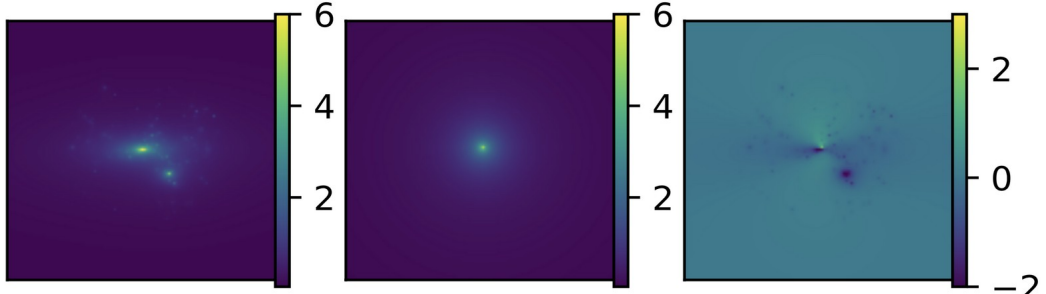


PIEMD+eNFW model. Fit of a NFW model.
Second clump present in projected density map

**PSZ2G228**

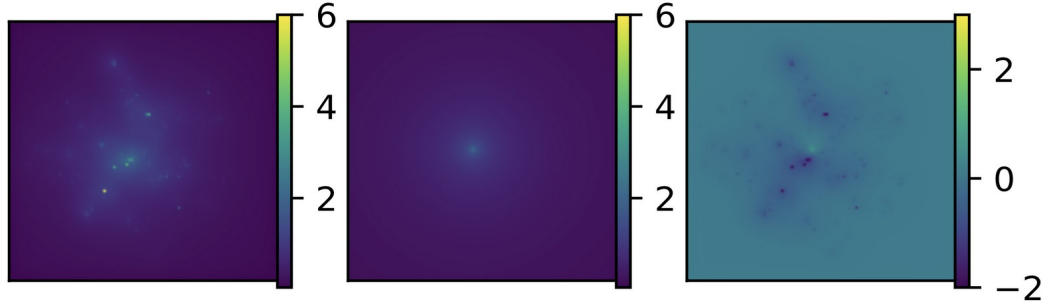


LTM model. Fit of a NFW model.
Complex morphology

**PSZ2G144**

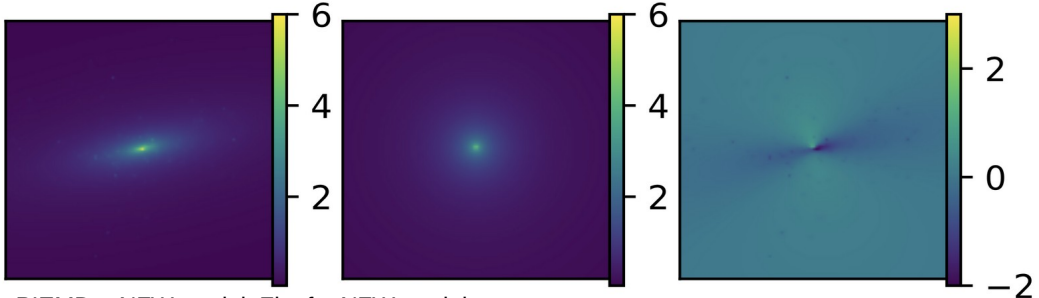


PIEMD+eNFW model. Fit of a NFW model.
No hints of the over-pressure

**MACSJ1424**

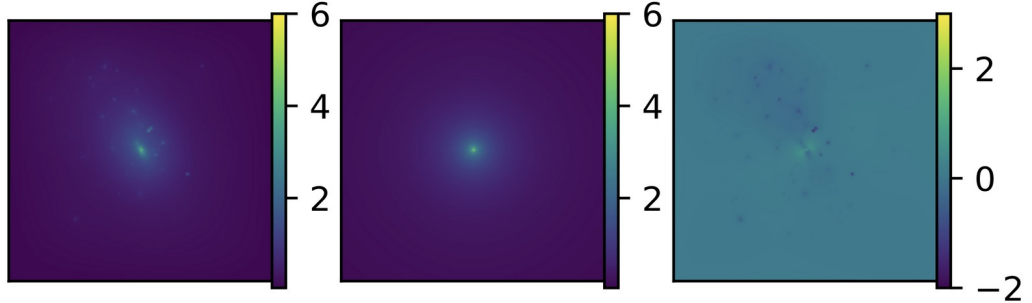


LTM model. Fit of a NFW model.

# Deflection

A distribution of matter with surface mass density $\kappa$ deflects the light an angle α


$$\nabla \cdot \vec{\alpha} = 2\kappa$$

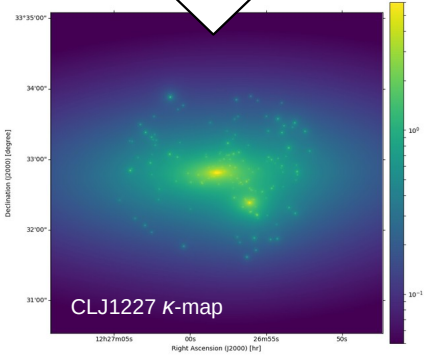


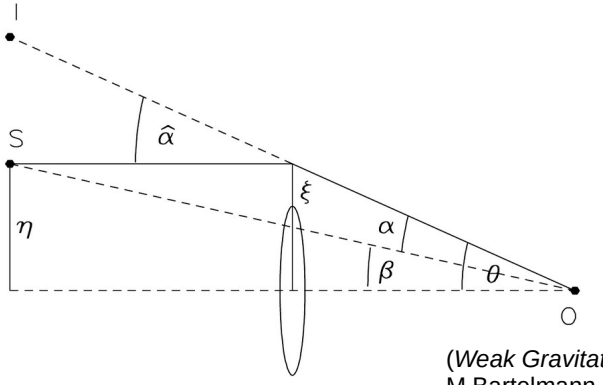


(*Weak Gravitational Lensing,* M.Bartelmann and P.Schneider, *2001*)

$$\vec{\beta} = \vec{\theta} - \vec{\alpha}(\vec{\theta})$$

Real position of the source

Observed position of the source